

OMAE2004-51236

DRAFT

CFD Analysis of Large Caisson Interaction with Current at Supercritical Reynolds Number

Subrata K. Chakrabarti, Offshore Structure Analysis, Inc., 13613 Capista Dr., Plainfield, Illinois, USA
Kristian K. Debus, Jonathan Berkoe and Brigette Rosendall, Bechtel Inc., 50 Beale Street, San Francisco, CA, USA

Abstract

The newly constructed Tacoma Narrows Bridge Piers represent large concrete floating caissons during their construction. For designing their mooring system the current force applied on the caissons in the Narrows must be known. The flow field around the caisson is highly complex and the calculation of the current load on the caisson by analytical means is difficult. On the other hand, model tests suffer from the distortion in the Reynolds number. Therefore, a two-prong approach was undertaken. Besides the fixed model test of the caissons for current forces, a CFD analysis of the flow around the caisson is chosen. A 3-D CFD approach is considered more appropriate than a 2-D one, since the bottom contour at the site is irregular and water depth is rather shallow.

This paper discusses the CFD method and the results obtained from such analysis. The numerical analysis was carried out in both ebb and flood flow of the tidal current in the basin. One of the difficulties of the computational method is very high Reynolds number encountered by the large current and large size of the caisson. The analysis was performed in both model and full scales so that the difference in the results may be investigated. Also, since the model test data was available, comparisons could be made between the CFD and model test results on the drag and lift forces on the caisson.

1. INTRODUCTION

A new suspension bridge is being constructed in the Tacoma Narrows, close to Seattle, Washington State. The new bridge is built just south of an existing bridge mounted on 2 caissons, referred to as East Caisson (Tacoma side) and West Caisson (Gig Harbor side). Each pier is about 80' wide and 130' long in plan. The caissons of the new bridge are in close proximity of the piers of the existing bridge. They experience large current in the ebb and flood flow through the Narrows.

It has been observed at the existing bridge that the vortices shed from the pier are directed downward, imposing a significant lift component to the loads on the pier and thus likely to do the same to caisson. It is also believed that the downward direction to the vortices is coupled to the transverse components of the vortex formation.

The transverse and lift loads on the caisson – particularly during the flood flow direction scenario in which the caisson lies in the wake of the existing pier – are significant and critically affect the stability of the structure. These loads are induced by the current flow adjacent to the caisson and also by the shedding and subsequent flow re-circulation of vortices in the wake region. The vortex shedding phenomena is explicitly transient (time-varying).

The Reynolds number of the flow around the caisson is on the order of 10^8 . This is an extremely high value, which has not been solved using a CFD approach. There is no literature available on this subject at such high Reynolds number. The implication of the high Reynolds number is the difficulty in predicting the flow separation and vortex shedding in the wake regions. The other key

implication of the high Reynolds number is that extremely tight meshing around the caisson/pier is required and thus an extremely (and potentially prohibitively) large model requiring long computation times.

Bearing in mind this limitation, the CFD analysis of the existing and new pier was made for a large number of cases. The software AcuSolve is employed to describe the flow field around the pier/caisson and forces on the caisson were derived numerically. This paper describes some interesting results and the feasibility of the CFD analysis for such high Reynolds number. Most of the CFD runs were made in full scale. However, a few runs were also made in model scale. This allowed a comparison of the results between the full and model scale so that any scale effect may be studied. Additionally, the time history data on the forces and moments generated by the 3-D CFD analysis are compared with the fixed body physical test data. The CFD results allowed a direct comparison with the model test results and provided some validation for the CFD model. This comparison established the accuracy of the CFD model at a Reynolds number of the order of 10^5 . The similarity and differences between the two and, in particular, the effect of the Reynolds number between the numerical and physical models are discussed.

It should, however, be noted that there is practically no data available in the literature on high Reynolds number (of the order of 10^8), which makes it difficult to assess the accuracy of the full-scale CFD results. The single CFD simulation of a bluff body indeed gave reasonable value for the drag coefficient.

In the real case, the new caisson is not fixed, but will move due to oscillating lift (as well as inline) loads experienced from the alternating vortex shedding from the caisson due to current flow. The CFD simulation will fail to duplicate this situation and the effect of moving caisson will remain an unknown.

There have been many studies that have examined the case of a uniform approach flow past a circular cylinder; one of the latest is Williamson (1996). The physics of the uniform flow problem is fairly well understood. Recent results by Lu et al. (1997), using the large eddy simulation (LES) method for Reynolds numbers to 44,200, reflect the present state of the art in doing 3D calculations for uniform flow past a circular cylinder. There have been several recent CFD studies, which have used the solution of the 2D Navier-Stokes equations to provide the input to ordinary differential equations to calculate the VIV oscillations of the cylinder. Meling (1998) used a 2D finite-element procedure, with the one equation turbulence model of Spalart and Allmaras (1992), to calculate the uniform flow past a cylinder at Reynolds numbers to 21,000. In spite of using the 2D description, Meling found excellent agreement between his calculated results and the experimental results of Moe, et al. (1994). Schulz & Kallinderis (1998) also used a 2D finite-element approach to describe the VIV behavior of a circular cylinder. Schulz & Kallinderis presented results for a Reynolds numbers as high as 4.75×10^5 , but without experimental corroboration.

An approach flow to a cylinder with axial shear is even more challenging than the uniform approach flow problem. When the current has a spanwise (axial) shear, the flow pattern around the cylinder is influenced by the secondary flow generated by the leading edge stagnation-pressure gradient. The secondary flow will influence the vortex shedding over the cylinder length. The vortex shedding is influenced by Reynolds number and shear parameter Du/U_o , where Du is the difference in velocity over the length of cylinder (or segment of length) and U_o is the freestream velocity determined by the average of the velocities over the cylinder span in question. Note that the upper part of the flow in the Narrows is reasonably uniform; but a large shear region remains near the bottom of the shallow Narrows. This is modeled in the 3-D CFD simulation.

2. CFD MODEL DESCRIPTION

It is recognized that the Large Eddy Simulation (LES) model can handle Reynolds number of about 10^5 . LES models are OK with shear layers but not boundary layers. On the other hand, the Reynolds-Averaged Navier-Stokes (RANS) models have been successful in handling boundary layers, but not shear layers. Therefore, it is assumed that a hybrid model will do better with both layers present. The commercial CFD solver Acusolve™ is based on the finite-element method (FEM), which directly computes the pressure on the body surface, and additionally allows for less mesh density in the boundary layers. AcuSolve solves the transient Navier Stokes equations using hybrid RANS/LES turbulence. The [Spalart-Allmaras (1992)] RANS model handles the upstream and the boundary layer turbulence conditions. In this case, flow separations will occur behind the caissons. Since the Reynolds number is very high, shedding is expected to be unsteady, where vortices are generated having a large free shear area. This is where the LES part of the model come into play, in which the vortices appear naturally from the solution of the Navier Stokes equations.

The problem is that there exist a number of different size vortical structures, considering the high Reynolds number of this problem. The smaller structures need modeling as accurately as possible, in order to get the proper cascade of energy from the large scale vortical structure to the small one. If the small ones are not modeled correctly, energy transfer will be incorrect and the large vortices will be in error. This is a major problem with the current state of turbulence modeling in CFD.

This, in reality, involves two problems: (1) having the correct (or a good) turbulence model (i.e., the proper mathematical model), and (2) accurately and efficiently solving the mathematical model. The finite element analysis, in mathematical model, the present formulation provides the most accurate solution. The stabilizing operators do not damp out the solution for robustness. It only adds

enough and in the direction needed to counteract the destabilizing effects of the convective and divergence free terms. Regarding the first item, this is still an open issue, and in opinion, will remain an open issue for decades.

2.1 Solution Methodology

The following transient turbulent incompressible Navier-Stokes equations are considered in the numerical analysis. They describe, respectively, the conservation of mass and momentum in three-dimensions.

$$\nabla \cdot \vec{u} = 0 \quad (1)$$

$$\rho \frac{Du}{Dt} = -\nabla p + \nabla \cdot \tau \quad (2)$$

where ∇ is the operator, \vec{u} is the velocity vector; ρ is the density; and p is the pressure. The first term of Eq. 2 is the material derivative; and τ is the stress tensor modeling the sum of contributions from the viscous and turbulence Reynolds stress,

$$\tau = (\mu + \mu_t)(\nabla u + \nabla^T u) \quad (3)$$

where μ and μ_t are the molecular and turbulent eddy viscosities, respectively. The one-equation RANS turbulence model [Spalart-Allmaras (1992)] models the eddy-viscosity with the Detached-Eddy Simulation (DES) modification. This model is written as

$$\frac{D\tilde{v}}{Dt} = c_{b1} \tilde{S} \tilde{v} + \frac{1}{\sigma} \left(\nabla \cdot (v + \tilde{v}) \nabla \tilde{v} + c_{b2} (\nabla \tilde{v})^2 \right) - c_{w1} f_w \left(\frac{\tilde{v}}{d} \right)^2 \quad (4)$$

where \tilde{v} is the unknown field. The definition of \tilde{S} and f_w and constants σ , c_{b1} , c_{b2} , and c_{w1} is given in Spalart (1997). The quantity \tilde{v} is closely related to the kinematic eddy viscosity. The turbulence eddy viscosity is given by

$$\mu_t = \rho \tilde{v} \frac{\chi^3}{\chi^3 + c_{v1}^3} \quad \chi = \rho \tilde{v} / \mu \quad (5)$$

The DES model is obtained by replacing the distance to the nearest wall, d , by

$$\tilde{d} = \min(d, C_{DES} \Delta) \quad (6)$$

Here Δ is a local measure of element size and C_{DES} is a constant. [See Spalart (1997) for details]

It is well known that RANS turbulence models can be very effective in resolving boundary layers and free-stream flows. However, they do a poor job in capturing free shears. On the other hand, LES turbulence models can be effective in capturing the free shear, while they need unattainable mesh resolution to capture boundary layers, especially at high Reynolds numbers. For well-generated meshes, DES is designed to naturally switch between RANS and LES where appropriate. The mesh spacing in the boundary layers is of the order of boundary layer thickness. Consequently, in the boundary layer, DES reverts to the ‘‘RANS mode’’ to predict the boundary layer and flow separations. Away from the walls, and when production and destruction terms are balanced, the length scale $\tilde{d} = C_{DES} \Delta$ of the model yields a Smagorinsky LES eddy viscosity $\tilde{v} \propto S \Delta^2$. In short, DES attempts to provide the best of both worlds.

The above equations constitute a system of five equations with five unknowns. These equations are solved using the Galerkin/Least-Squares finite element technology [see Hughes (1987)] and references therein for in-depth description. Equal-order nodal interpolations for all working variables, including pressure, are used with low-order elements. Moreover, the semi-discrete generalized- α method of Hulbert (1993) is used to resolve the time dependencies. The Galerkin finite element formulation provides the base algorithm. Galerkin formulation, which is equivalent to the central difference formulation in finite differences, does not yield stable discretization for the solution of the incompressible Navier-Stokes equations. The stability difficulties arise from two main sources: (1) the divergence-free constraint, i.e., the continuity equation; and (2) the convective term in the momentum equations. The least-squares operator is designed to add the needed stability without sacrificing accuracy. AcuSolve improves performance in three ways: (1) it solves the coupled velocity/pressure system, yielding substantially faster convergence; (2) its architecture has been implemented from the ground up for vector and cache-based super-scalar machines; (3) it is designed for coarse-grain parallel machines. Domain decomposition is used to break and distribute the elements and nodes to different processors. Message Passing Interface (MPI) is used to communicate between the processors. All the algorithms are designed specifically to perform on coarse-grain parallel machines.

2.2 Model Geometry and Bathymetry

The CFD model was set up as a rigid body system submerged in water. The complex bathymetry (based on actual mapping of the riverbed) was imported to the meshing tool from a CAD model. The bathymetry data was converted using Microstation (Bentley, Inc.) to a surface model suitable for export to the CFD meshing software. Separate models were created for the East and West piers. Each of these models extended sufficient distance into the channel to allow for specification of far-field boundary condition.

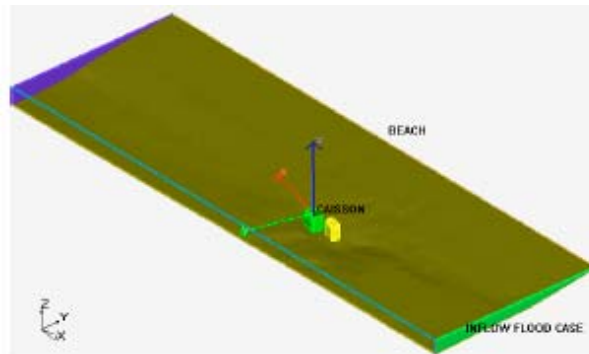


Figure 1: Computational domain for the West Side with bathymetry and pier/caisson configuration

Figure 1 shows the West pier model including the surface bathymetry, caisson/pier configuration, boundary locations, and coordinate system orientation.

An unstructured hybrid mesh with tetrahedral and prismatic elements for the boundary layers was created using the Tetra module of the ICEM-CFD software (ANSYS, Inc.). To reduce run time and memory usage the prismatic elements were converted to tetra, leading to a mesh size of approximately 3.5 million elements. Figure 2 shows a plot of the mesh around the new caisson with the prismatic elements on the caisson surface. The mesh density was increased in the wake region behind the caisson to optimize grid resolution and capture the vortex shedding and re-circulation areas.

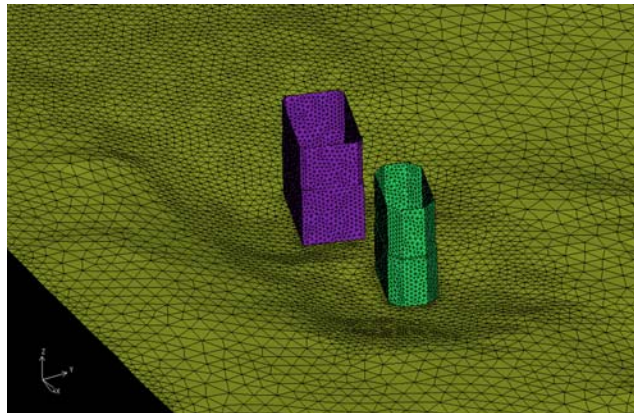


Figure 2: Computational mesh with prismatic elements on the caisson and pier

2.3 Boundary Conditions

Simulations were carried out for 9 different scenarios at the East and West piers under ebb and flood conditions. Maximum current velocities for the Tacoma Narrows considered were flow speeds of 9 knots (4.6 m/s) at the East piers and 7 knots (3.6 m/s) at the West piers. Maximum flows were used to provide the ‘worst case scenario’ data. The far-field side boundaries and the water surface boundary were set as symmetry boundaries. For the ebb direction, a uniform velocity of 3.6 m/s was applied at the inlet boundary.

2.4 Computer Simulations

All simulations were run on a Compaq ES40 server using four 667 MHz Alpha processors running in parallel and equipped with four gigabytes (GB) of memory (RAM). The runs were typically initialized by computing an approximate steady state solution, and then running in transient mode for many cycles until repeatability in the solution behavior (based on both forces and drag coefficients) was observed. The computation time varied depending on the model size and flow conditions, but typically required about four days.

3. CFD MODEL VALIDATION

The first step for the CFD model was to run benchmark simulations and compare the results to measured data for standard similar bluff body configurations such as circular and square cylinders. The case of the circular cylinder at a high Reynolds number of 10^8 was chosen for the CFD run to spot check accepted drag coefficients of circular cylinders. The results show a mean C_D value of about 0.72. It is close to the published value of 0.78 at $Re = 10^7$, even though the published values do not extend beyond this value of Re .

The Reynolds numbers evaluated ranged from $Re = 10^5$ in model scale up to $Re = 10^8$ (full scale) into the super critical flow regime. The results for drag coefficients and Strouhal numbers were in excellent agreement for the square cylinder with a mean value close to 2.0 measured by Delany (1953). The details of these data may be found in Debus, et al. (2003). Since the modeling of flow separation around square cylinders is more repeatable (and numerically more robust) than for circular cylinders, extrapolation to higher Reynolds numbers from the limited range of available data was done with greater confidence.

4. SUMMARY OF CFD RESULTS

CFD analysis of the existing and new pier was made for a large number of cases. These include both the east and west piers. The caisson draft chosen are 61-ft, 120-ft and 140-ft. The run length varied from about 300 to 700 seconds. Most of the CFD runs were made in full scale. However, a few runs were also made in model scale. This allowed a comparison of the results between the full and model scale so that any scale effect may be studied.

A 3-D flow field for the west caisson in the presence of existing pier in a flood flow is given in Fig. 3.

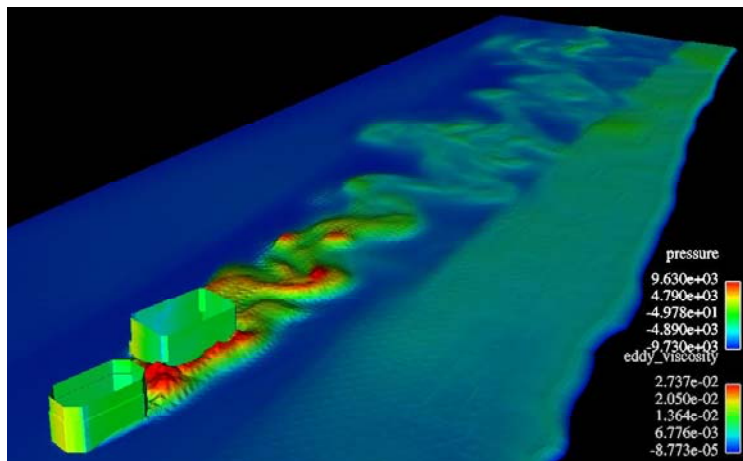


Figure 3: Flow visualization by CFD for West Caisson Flood Case @ 25 hours

The results of the CFD analysis are extensive. Here only a few sample results are presented. Since the analysis was performed for the east and west piers cases, results showing the comparison of the two are presented here. The case chosen is the ebb flow past the 120-ft draft caisson in 7-knot current. The X and Y forces are presented in Figs. 4 and 5.

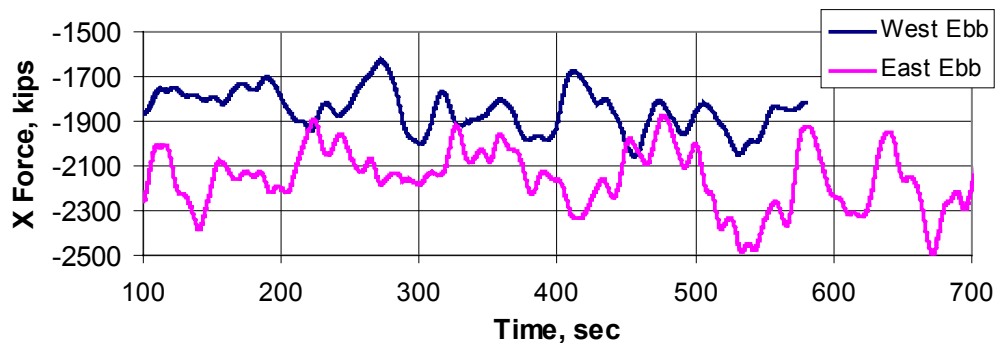


Figure 4: X Force on the New Caisson of 120-ft draft in 7 knot Ebb flow

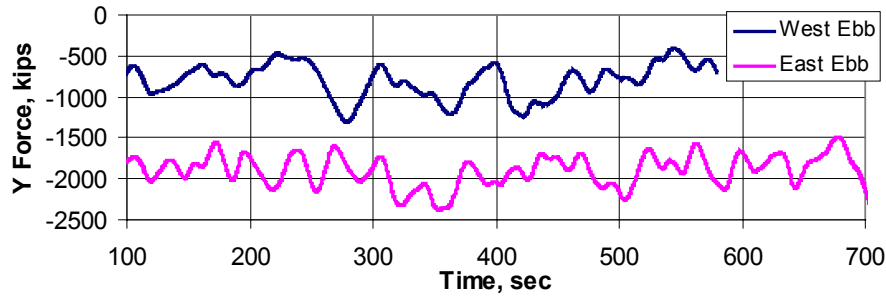


Figure 5: Y Force on the New Caisson of 120-ft draft in 7 knot Ebb flow

Note that the inline drag force as well as transverse force is higher for the East Pier than those for the West. Even though the pier geometry is equivalent, there are several differences in the bottom geometry between the East vs. the West. Water depth is greater on East Side. Also, the bathymetry shows higher curvature on East Side, which could affect flow direction and increase forces in the transverse direction. On the West Side the pier is closer to the beach where the water is shallower, on the East Side the caisson is closer to the beach. Larger gap/distance between the 120ft caisson and the riverbed reduces wall (no-slip condition) effect of bathymetry and yields higher velocities on lower end of caisson. Mass flow of current on East Side is approximately 1.5 times the West Side

5. COMPARISON OF MODEL vs. FULL-SCALE CFD FORCES

The CFD model was run for the same conditions in the model and full scales. The example chosen was the 143-ft draft caisson fixed on the East Side in the ebb and flood flow for a current speed of 7 knots. The purpose is to investigate the difference in the results for the two Reynolds number regimes. Note that the model Reynolds number is of the order of 10^5 while the full scale Reynolds number is about 10^8 .

The average values of the forces in the x, y and z directions are obtained from the CFD results for the two cases and are shown in the Table 1. The model results have been scaled up by the use of Froude scale for the purpose of comparison. It is clear that the average forces in all directions are about the same between the model and the prototype. The largest difference in the y-force of about 14 percent is still considered acceptable for the purpose of determining the scale effect.

Table 1 Mean Forces on Caisson in Model and Full Scale

Ebb flow 140 ft	Model, kips	Full-scale, kips	% difference
Average x Force	-1449	-1424	-1.7
Average y Force	-1360	-1382	1.6
Average z Force	-666	-588	-11.7
Flood flow 140 ft	Model, kips	Full-scale, kips	% difference
Average x Force	23	20	-13
Average y Force	789	903	14
Average z Force	-603	-675	-12

The data sample for the time history simulation was limited (about 300 sec) to compare the maximum values or to obtain the PSD of the time series accurately. However, the time history between the scaled up model data and the full-scale CFD simulation are plotted in Figs. 6-9. Figures 6 and 7 show the X and Y forces for the ebb flow. The flood flow case is shown in Figs. 8-9. From this comparison the following trends may be observed.

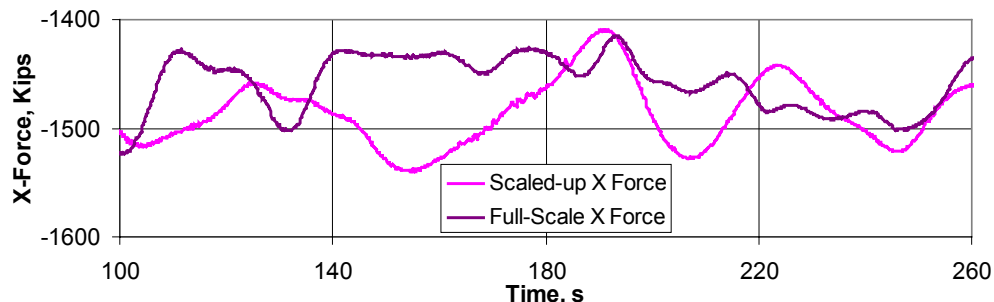


Figure 6: Time History of X Forces for Model and Prototype Ebb Case

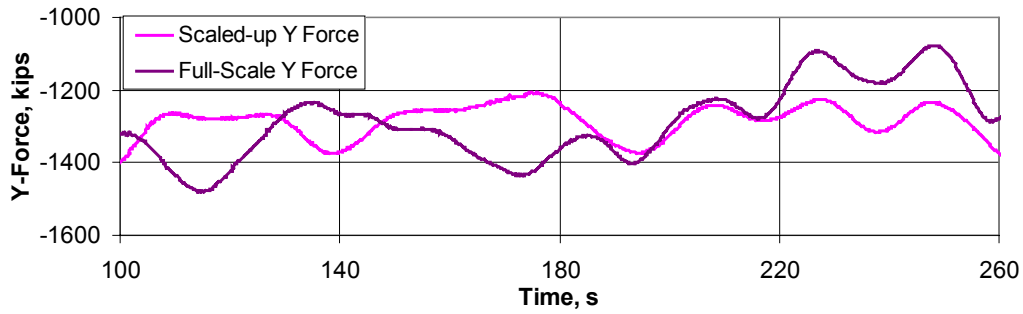


Figure 7: Time History of Y Forces for Model and Prototype Ebb Case

The magnitudes of the forces in x, y and z directions for the ebb flow case are very similar once the downward or upward slope in the data is ignored. The frequency contents in the model and prototype forces are very close to being the same. This is an important conclusion since this means that the vortex shedding process in the lower Reynolds number range for the model is about the same as that of the prototype. This is so because both are in the turbulent region and the rectangular shaped caisson having sharp edges has fixed shedding zones.

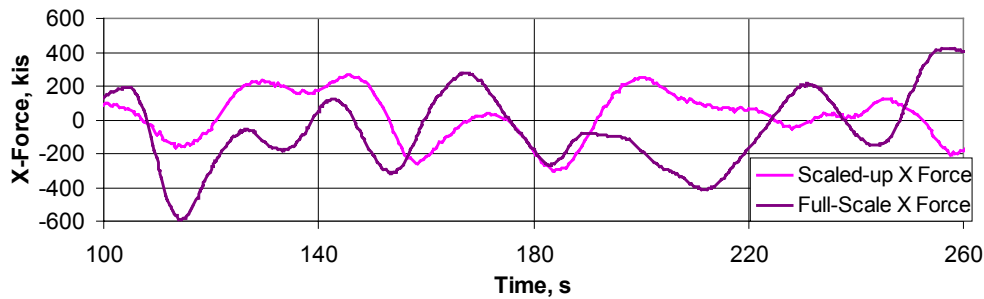


Figure 8: Time History of X Forces for Model and Prototype Flood Case

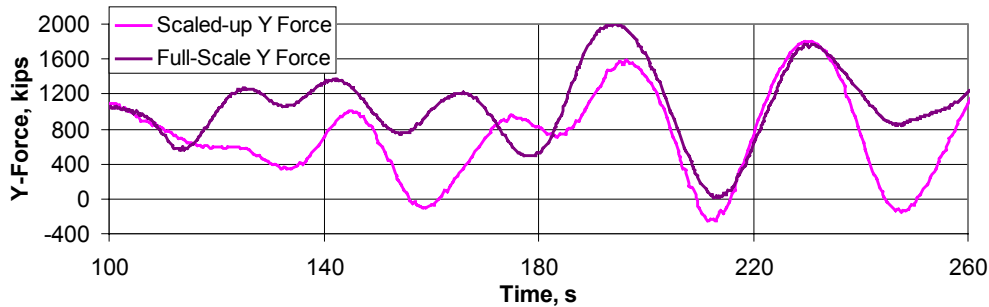


Figure 9: Time History of Y Forces for Model and Prototype Flood Case

The same conclusions may be drawn for the flood case for the same run with the possible exception of the z force. In this case the dynamic model appears to have higher magnitude compared to the corresponding prototype force. However, the CFD x and y forces are even more similar between the scaled model and prototype cases.

It appears from the CFD simulation that the scale effect due to Reynolds number is quite small. The high frequency contents of the force could not be verified as the CFD does not include this part of the force component. However, the force data from the fixed caisson model tests shows a broad band spectrum for the x and y forces. Since the model forces are similar to white noise, it is anticipated that the full-scale forces will have the similar characteristics and the frequency content must be similar. Of course, the effect on magnitudes cannot be concluded from this observation.

6. COMPARISON OF CFD ANALYSIS AND MEASUREMENT OF FORCES ON CAISSON

The time history data generated by the 3D CFD analysis shows the forces and moments on the 140-ft draft caisson in 7 knots current in ebb flow for a time length of about 300 sec. The HRW rigid body test data provides the forces on the 143-ft draft caisson making it possible to compare the two cases. The mean values of the forces in the X, Y and Z directions are compared in Table 2. Note that the

mean forces for the ebb flow at the 7-knot speed match quite well. the mean forces in the flood flow at the 9-knot speed are not predicted by the CFD results well. Note however, that the magnitudes of the mean forces in the flood flow are small due to the blockage of flow from the existing pier and the difference in the two cases may not be as significant.

Table 2: Summary of Mean Forces by CFD Analysis and HRW Tests

	X-F	Y-F	Z-F
120ft East Caisson		7 knots	Ebb
Mean F HRW	-1837	-2032	-1099
Mean F CFD	-2152	-1872	-1117
120ft East Caisson		9 knots	Flood
Mean F HRW	-342	1297	-825
Mean F CFD	-68	929	-612

In order to examine the dynamic forces, the case of 143-ft caisson in 9-kt flood current was chosen. The dynamic part of the force obtained from the CFD analysis is shown in Fig. 10 for the inline (surge), and transverse (sway) force overlaid on the measured forces. The low frequency part of the dynamic forces appear to be reasonably similar between the CFD and measured forces. It is clear, however, that the CFD force on the caisson is deficient in describing the high frequency contents present in the measured rigid body forces. The oscillating CFD force is primarily at low frequencies corresponding to a Strouhal number of about 0.2.

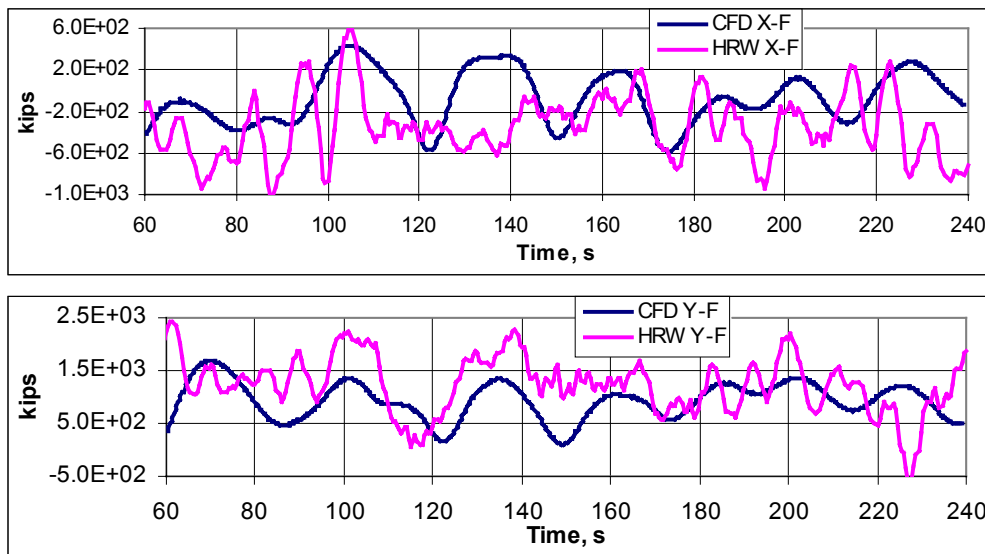


Figure 10: CFD vs. HRW Force Time History – 143 ft Caisson in 9 kts Flood

This is clearly evident in the PSD plots of the two forces in Fig. 11 in which the frequency distribution of the forces are shown. The high frequency contents found in the measured forces are absent in the CFD analysis results. This area of energy generally excited the caisson in its dynamic motion and is necessary to compute the line tension correctly.

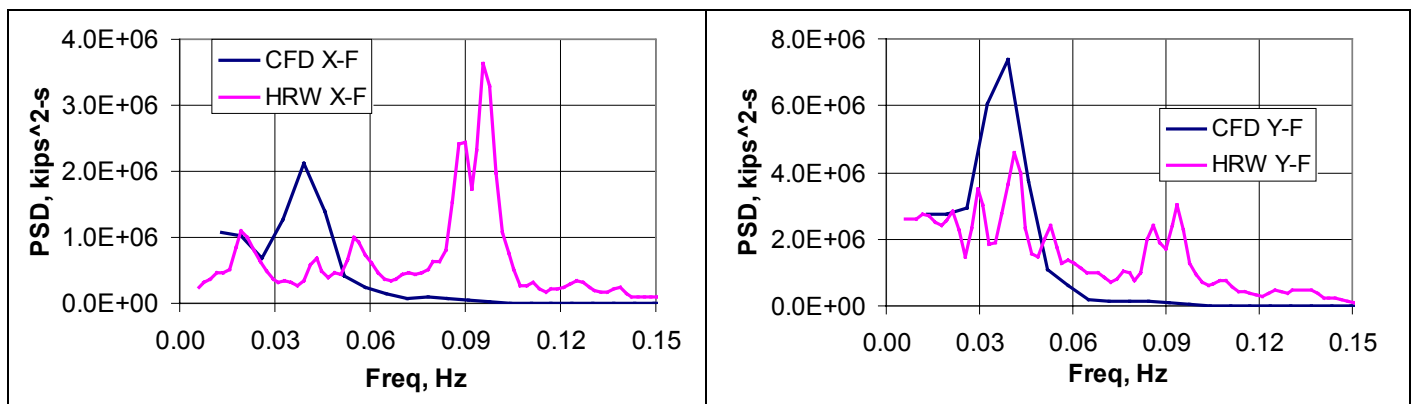


Figure 11: CFD vs. HRW Force Spectra – 143 ft Caisson in 9 kts Flood

The comparison is also shown for the case of ebb flow for the 123-ft caisson in 7-kt current in Figs. 12 and 13. The time history is shown in Fig. 12 with the corresponding PSD results in Fig. 13. As found for the mean steady forces, the east caisson is exposed to current in ebb flow and therefore, the steady loads are much higher in this case compared to the flood flow. Accordingly, the dynamic force components are relatively lower in the high frequency range. However, similar conclusions as above may be drawn even here. The high frequency component, albeit small, shows up in the measured forces on the fixed caisson, which is absent in the CFD results. Therefore, even though the high frequency dynamic component is smaller compared to the steady force component, it is absent in the CFD analysis.

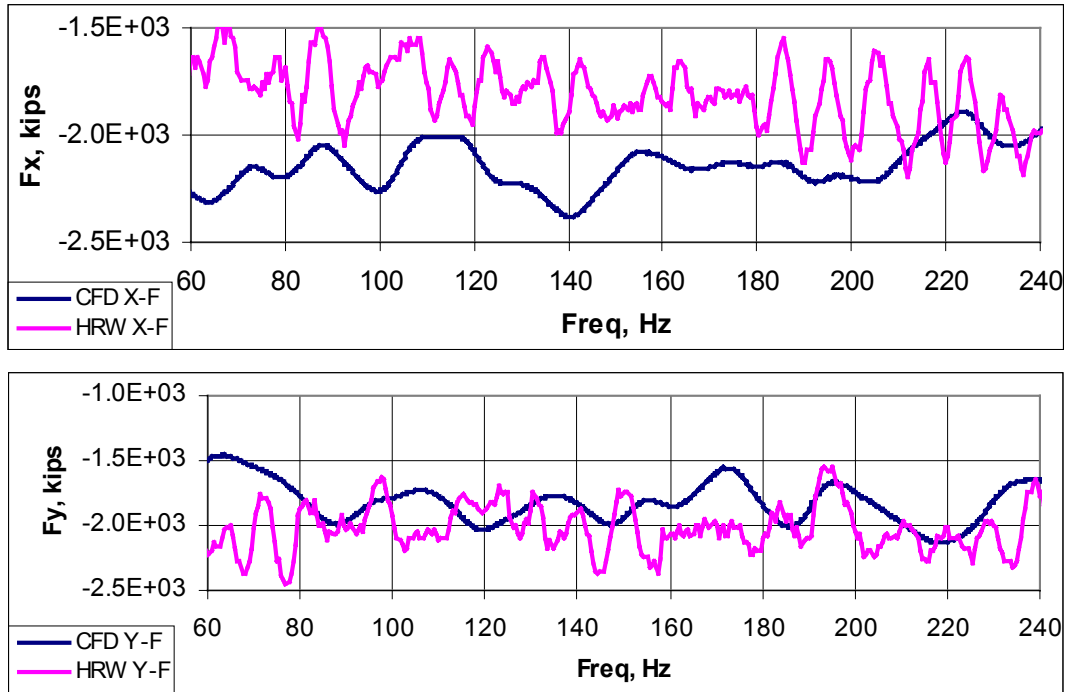


Figure 12: CFD vs. HRW Force Time History – 123 ft Caisson in 7 kts Ebb

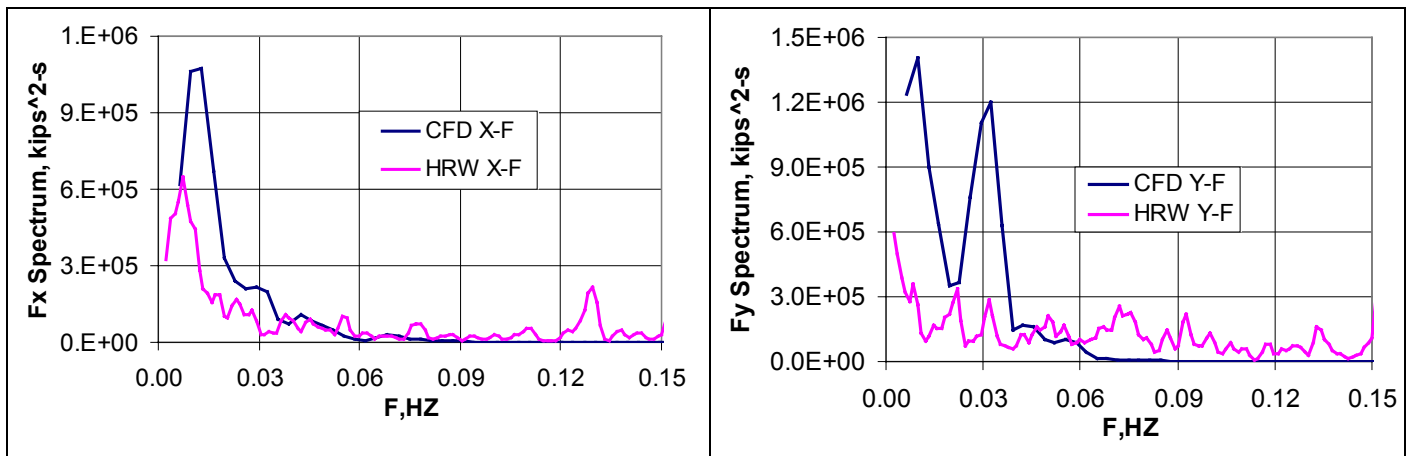


Figure 13: CFD vs. HRW Force Spectra – 123 ft Caisson in 7 kts Ebb

This deficiency in the CFD analysis is its inherent difficulty in amply describing the local flow field due to strong current at high Reynolds number. It appears that the CFD results describe the broader flow field around the caisson reasonably well and is even able to give reasonable steady load prediction. However, the local variation and vortex field does not appear to be picked up adequately by the CFD model even after the numerical sophistication introduced. It is probably due to the fact that the finite element description of the local flows close to the caisson surface is not fine enough. In order to obtain a better flow description close to the caisson, possibly a DNS approach is required as opposed to the hybrid approach taken here. This is, possibly, beyond the state of the art for now.

7. CONCLUSIONS

The Tacoma Narrows Bridge Expansion Project presents a good example of the value of CFD modeling. At first glance the bridge caisson design would appear to be far less of a challenge from a fluid dynamic standpoint than an aircraft or ship. However, the Reynolds numbers involved in this case are extraordinarily high, such that neither relevant scale model data nor proven design correlation is readily available.

In recognizing the challenge due to the high Reynolds number, unsteady nature of the flow, and degree of accuracy required for fluid-structure force calculations, a unique commercial solver package AcuSolve, based on a hybrid RANS/LES turbulence model (referred to as DES) and the finite element methodology was employed.

The results were found to be quite sensitive to the water depth and bathymetry. It is clear that a 2-D simulation will yield completely erroneous results in this case. They provided valuable information on the flow pattern around the bluff caisson and gave qualitative information on the effect of the Strouhal frequency on the forces on the caisson.

The model and full scale CFD analysis gave similar results on force for the steady and low frequency forces. The difference in the Reynolds number was a factor of 1000 in this case. This is an important observation, even if the high frequency forces remain uncorrelated by the CFD.

The CFD results were found to provide reasonable steady and low frequency large eddy forces when compared to the corresponding experimental data. The method appears applicable to static and pseudo-dynamic problems even in supercritical flows. This is a very important finding since the Reynolds number encountered in these problems exceed any known such results in the published literature.

The CFD model, however, failed to duplicate the high frequency vortex-shedding frequencies in the X and Y forces. This is primarily due to limit in the meshing sizes in the near vicinity of the caisson/pier.

REFERENCES

Hughes, T.J.R., "Recent Progress in the Development and Understanding of SUPG Methods with Special Reference to the Compressible Euler and Navier-Stokes Equations," *Int. J. Numer. Methods Fluids*, 1261-1275 (1987).

Chung, J. and Hulbert, G.M. "A time integration algorithm for structural dynamics with improved numerical dissipation: The generalized- α method", *J. Appl. Mech.* 60 371-75, (1993).

Spalart, P.R. and Allmaras, S.R., "A One-Equation Turbulence Model for Aerodynamics Flows," AIAA Paper No. 92-0439, 1992.

Spalart, P.R. Jou, W.H. Strelets, M. and Allmaras, S.R. "Comments on the Feasibility of LES for Wings, and on Hybrid RANS/LES Approach" *Advances in DNS/LES*, 1st AFOSR Int. Conf. on DNS/LES, Greyden Press, Columbus OH, Aug. 4-8, 1997.

Meling, T.R. (1998), "Numerical Prediction of the Response of a Vortex-excited Cylinder at High Reynolds Numbers", *Proc. of the 17th ASME Conference on Offshore Mechanics and Arctic Engineering*, Lisbon, OMAE paper no. 98-0315.

Moe, G., Holden, K. and Yttervoli, P.O. (1994), "Motion of Spring-supported Cylinders in Subcritical and Critical Water Flows", *Proc., Fourth International Offshore and Polar Engineering Conference*, 468-475.

Schultz, K. and Kallinderis, Y. (1998), "Numerical Prediction of Vortex-induced Vibrations", *Proc. of the 17th ASME Conference on Offshore Mechanics and Arctic Engineering*, Lisbon, OMAE paper no.98-0362.

Smagorinsky, J. (1963)," General Circulation experiments with the primitive equations; I, Basic experiments", *Monthly Wea. Rev.*, 91, 99-164.

Spalart, P.R. and Allmans, S.R., " A one-equation turbulence model for aerodynamic flow", AIAA paper no. 92-0439, Reno, NV, 1992.

Williamson, C.H.K. (1996)," Vortex Dynamics in a Cylinder Wake", *Ann. Rev. Fluid Mech.*, 28, 477-539.

Debus, K., Berkoe, J., Rosendall B., and Shakib, F., "Computational Fluid Dynamics Model for Tacoma Narrows Bridge Upgrade Project", 4th ASME/ JSME Joint Fluids Engineering Conference, FEDSM2003-45514, Honolulu, Hawaii, July, 2003